Applied Energy 228 (2018) 891–901

Contents lists available at ScienceDirect

Applied Energy

journal homepage: www.elsevier.com/locate/apenergy

Parametric study and flow rate optimization of all-vanadium redox flow batteries

Dong Kyu Kim[c], Sang Jun Yoon[b,d], Jaeho Lee[a,d], Sangwon Kim[a,d,*]

[a] KIST Europe, Korea Institute of Science and Technology Europe, Campus E71, Saarbrücken 66123, Germany
[b] Center for Membranes, Korea Research Institute of Chemical Technology, Daejeon 34114, Republic of Korea
[c] School of Mechanical Engineering, Chung-Ang University, Seoul 06974, Republic of Korea
[d] Transfercenter Sustainable Electrochemistry, Saarland University, Saarbrücken 66125, Germany

HIGHLIGHTS

- Performance and efficiency of all-vanadium redox flow batteries were studied.
- Relationship between ion concentration and parameters in the system was analyzed.
- Steady state and transient responses established an optimal operating strategy.
- An empirical equation is suggested to maximize the energy efficiency of the systems.

ARTICLE INFO

Keywords:
All-vanadium flow battery
Numerical analysis
Ion concentration
Flow rate
Operating strategy

ABSTRACT

The parametric study for an all-vanadium redox flow battery system was examined to determine the optimal operating strategy. As dimensionless parameters, the stoichiometric number and state of charge were used to apply the strategy to all scales of the flow battery system. In this study, we developed a transient model for this system, which is supported by experimental data, to analyze effect of parameters on the ion concentration and determine its optimal operating conditions. First, the performance of the flow battery system was analyzed in steady-state conditions to examine the changes of the ion concentration depending on different flow rates, current densities, and sizes of active area. As flow rate increases, the energy efficiency slightly increases, because faster flow rates can deliver more vanadium ions from the reservoir. The energy efficiency decreases according to current density, because large current results in large amount of ohmic loss of membrane. When the size of active area increases, the energy efficiencies remain constant, however, the cycle time decreases. Next, the transient response for the system was analyzed by changing the stoichiometric number and current density during the charge and discharge processes. Variation of the system's energy efficiency was studied with changes in the stoichiometric number and state of charge as the current density was varied from 20 to 100 mA/cm^2. Increasing the flow rate at the beginning of the charge–discharge process is more efficient in the low current density region. At a current density of 100 mA/cm^2, however, it is better to increase the flow rate after the state of charge reaches 50%. Lastly, an operating strategy is suggested that involves controlling the mass flow rate of the electrolyte during the charge–discharge process. The operating strategy is presented as an empirical equation defined by the stoichiometric number and state of charge. Notably, this equation can contribute to improving the performance of all scales of the flow battery system by simply changing the electrolyte flow rate at right time.

1. Introduction

Large-scale energy storage systems (ESSs) are a promising solution to ease the problems associated with intermittent power delivered from renewable energy sources such as wind and solar energy. All-vanadium redox flow batteries (VFBs) have received considerable attention as a candidate for large-scale ESSs due to their long cycle life, flexibility for scale-up, quick response, and low maintenance cost [1,2]. However, many performance challenges of VFBs required by the market persist; low ion selectivity of the membrane, low energy density, and a lack of studies on its optimization have limited further commercialization of this type of flow battery [3].

* Corresponding author at: KIST Europe, Korea Institute of Science and Technology Europe, Campus E71, Saarbrücken 66123, Germany.
E-mail address: sangwon.kim@kist-europe.de (S. Kim).

https://doi.org/10.1016/j.apenergy.2018.06.094
Received 19 December 2017; Received in revised form 16 June 2018; Accepted 19 June 2018
Available online 06 July 2018

Many researchers have attempted to improve the performance of VFBs by developing materials. Some researchers tested high voltage redox pairs of vanadium/vanadyl acetylacetonates and Zn/Ce as an electroactive material to develop safe and high voltage aqueous redox flow battery system [4]. Other researchers tried to increase operating current density through KOH-activated carbon electrode [5,6]. Others developed dense polybenzimidazole membranes that has highly proton conductive and low vanadium permeability to increase energy efficiency [7]. On the other hand, there are researches to improve performance of the VFB system by distributing the electrolyte uniformly in the electrode. Some studies compared the flow field for flow-through channel and flow-by channel [8,9], and other studies investigated flow field in various designs of flow channel [10]. Others explained the importance of the compression force for mass transport of the electrolytes [11]. Others analyzed variation of ion concentration by considering mobility of ions [12] and develop an estimator to monitor capacity loss [13,14]. Unfortunately, relatively few studies have examined the effect of operating conditions on the performance of VFB systems.

Few studies have been conducted to improve performance by changing operating conditions. Some studies tried to reduce capacity fade by altering charging and discharging currents [15]. Other studies have attempted to maintain the operating temperature to prevent thermal precipitation in the cell by controlling the flow rate [16,17]. Others suggested operating strategies to increase the performance of VFB systems by changing the electrolyte flow rate [18]. Although a few studies have reported the effect of operating condition on the performance of VFBs, the lack of quantitative and transient analysis makes it difficult to utilize previous results to develop an optimal operating strategy for individual systems. Moreover, the present data remain insufficient to explain the relationship between the ion concentration and operating parameters in transient state.

In this study, we analyze the steady-state and transient responses of a VFB system and suggest an optimal operating strategy to maximize its performance for various current density by controlling the flow rate during the charge–discharge process. The discussion begins with an explanation of the steady-state results with experimental and numerical analyses to understand the changes of the ion concentration depending on different mass flow rates, current densities, and sizes of active area. Next, the effect of changing the flow rate and current density on the ion concentration change during the charge and discharge processes is investigated in order to observe the transient behavior of the VFB system. Then, the effect of the flow rate change under various states of charge is studied to understand the relationship involving the flow rate, state of charge, and current density. Lastly, the obtained results are considered in the development of operating strategies for maximizing the energy efficiency of VFB systems.

2. Methodology

A VFB system is mainly composed of a pump, reservoir, and stack, as shown in Fig. 1. Electrolytes are stored in each reservoir and pumped into the cells, which determines the battery's power via electrochemical reactions; $V^{2+/3+}$ and $V^{4+/5+}$ solutions are stored in the reservoirs and circulated in the negative and positive sides, respectively. The standard voltage of the VFB is 1.25 V, which is produced by reactions at the anode and cathode. At the positive electrode:

$$VO^{2+} + H_2O - e^- \underset{\text{discharge}}{\overset{\text{charge}}{\rightleftharpoons}} VO^{2+} + 2H^+ \quad E^0 = 1.00\ \text{V} \ \ vs.\ \text{SHE} \tag{1}$$

At the negative electrode:

$$V^{3+} + e^- \underset{\text{discharge}}{\overset{\text{charge}}{\rightleftharpoons}} V^{2+} + \quad E^0 = -0.26\ \text{V} \ \ vs.\ \text{SHE} \tag{2}$$

In this study, a model for VFB is developed and experimentally validated to analyze the steady and transient responses. We calculated the concentrations of each species at the electrodes and reservoir to obtain the performance of the VFB system. To consider transient mass transport phenomena within the VFB system, the mass transport of species, electrochemical reactions during the charge–discharge process are also included. Additionally, power consumption of pump is calculated to evaluate VFB system performance. The flow chart for VFB system model is presented in Fig. 2. Furthermore, the experimental setup was prepared to substantiate the developed model and determine an optimal operating strategy.

2.1. Modeling

We developed a VFB system model to examine the steady and transient responses with reference to previous studies. The stack and reservoir model is developed in quasi one-dimensional dimensional to analyze variation of state of charge (SOC) between inlet and outlet. An isothermal condition is assumed in the entire system. Furthermore, crossover of vanadium ions and water molecules are considered, and possible side reactions are considered, as well.

First, the concentrations of vanadium ions at each electrode were quantified using mass conservation equations [19]. Self-discharge reactions across the membrane due to concentration gradients were also considered to explain the effect of the operating parameters on the VFB efficiency [20]. At the positive electrode, V^{2+} and V^{3+} ions diffuse from the negative side and react with ions in the catholyte:

$$V^{2+} + 2VO_2^{+} + 2H^+ \rightarrow 3VO^{2+} + H_2O \tag{3}$$

$$V^{3+} + VO_2^{+} \rightarrow 2VO^{2+} \tag{4}$$

$$V^{2+} + VO^{2+} + 2H^+ \rightarrow 2V^{3+} + H_2O \tag{5}$$

At the negative electrode, reactions occur in the anolyte with VO^{2+} and VO_2^{+} ions that diffuse from the positive electrode:

$$VO^{2+} + V^{2+} + 2H^+ \rightarrow 2V^{3+} + H_2O \tag{6}$$

$$VO_2^{+} + 2V^{2+} + 4H^+ \rightarrow 3V^{3+} + 2H_2O \tag{7}$$

$$VO_2^{+} + V^{3+} \rightarrow 2VO^{2+} \tag{8}$$

Since the products of side reactions (5) and (8) can react repeatedly with VO^{2+} and V^{2+} in reactions (4) and (6), we have neglected V^{3+} and VO^{2+} generated from those reactions in our model [20]. Here, we assumed that the ions are circulated between the reservoir and stack by convection and are transported through the membrane by diffusion [21]. Based on the above explanation, concentration changes of V^{2+} and V^{3+} at the negative electrode during charge can be expressed as follows:

$$\varepsilon V_e \frac{dC_{V(II)}}{dt} = Q(C^{res}_{V(II)} - C_{V(II)}) + A_s \frac{j}{F} - \frac{A_m}{t_m}(D_2 C_{V(II)} + 2D_5 C_{V(V)} + D_4 C_{V(IV)}) \tag{9}$$

$$\varepsilon V_e \frac{dC_{V(III)}}{dt} = Q(C^{res}_{V(III)} - C_{V(III)}) - A_s \frac{j}{F} - \frac{A_m}{t_m}(D_3 C_{V(III)} - 3D_5 C_{V(V)} - 2D_4 C_{V(IV)}) \tag{10}$$

Here, ε is porosity; V_e is the electrolyte volume; C_i^{res} and C_i are the concentrations of the vanadium species at the reservoir and the VFB cell, respectively; Q is the flow rate; j is the current density; A_s is the active surface area for the reaction, which is written as SV_e, where S is the specific surface area for the reaction and is used as a fitted parameter; $A_m$is the membrane area; $t_m$is the membrane thickness; and D_i is the diffusion coefficient for each species, which is listed in Table 1. Concentration changes at the positive side during charge can be expressed as:

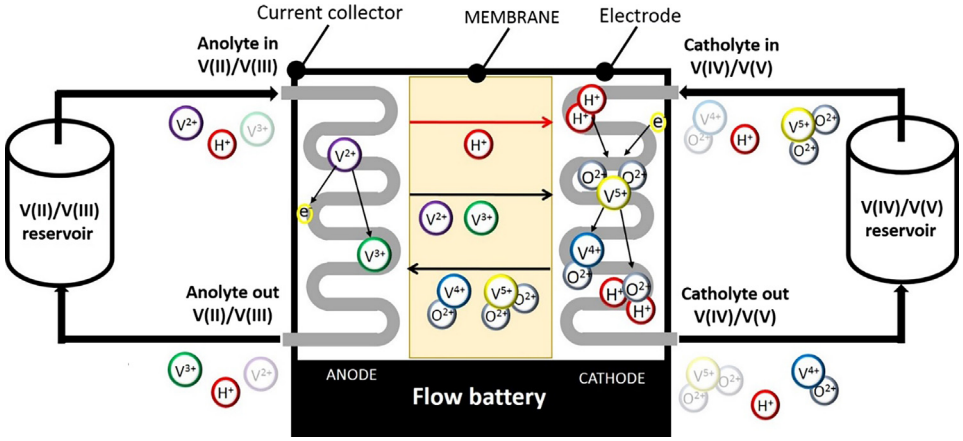

Fig. 1. Schematic diagram of all-vanadium flow battery.

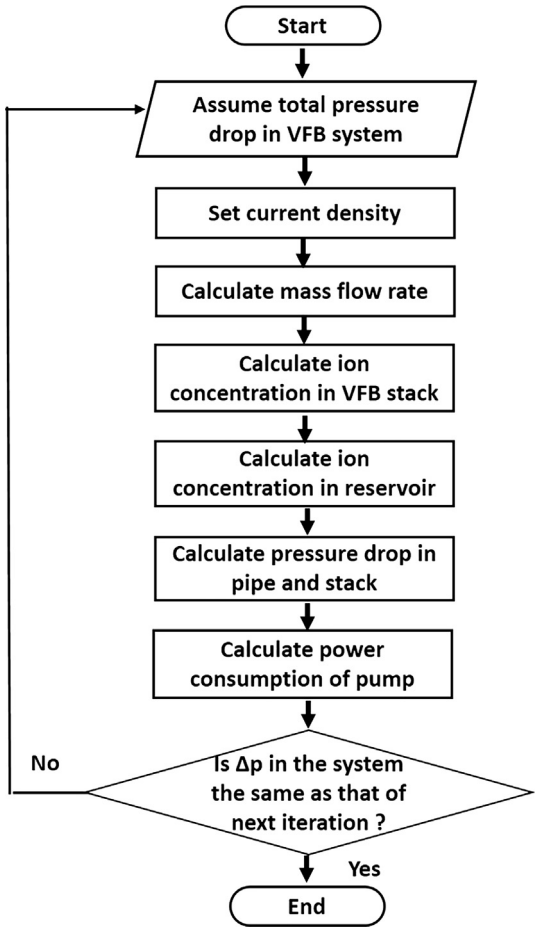

Fig. 2. Flow chart for VFB system model.

$$\varepsilon V_e \frac{dC_{V(IV)}}{dt} = Q(C^{res}_{V(IV)} - C_{V(IV)}) - A_s \frac{j}{F} - \frac{A_m}{t_m}(D_4 C_{V(IV)} - 3D_2 C_{V(II)} - 2D_3 C_{V(III)}) \quad (11)$$

$$\varepsilon V_e \frac{dC_{V(V)}}{dt} = Q(C^{res}_{V(V)} - C_{V(V)}) + A_s \frac{j}{F} - \frac{A_m}{t_m}(D_5 C_{V(V)} + 2D_2 C_{V(II)} + D_3 C_{V(III)}) \quad (12)$$

The concentration of protons at the negative electrode is obtained by considering the circulated electrolyte between the reservoir and stack in terms of electrode chemical reactions. At the positive side, the proton concentration can be expressed by considering the additional proton generation from oxidation reactions. To understand the variation of ion concentration in the electrode, the electrolyte velocity, u, is examined using Darcy's law.

$$\rho_{electrolyte} \frac{\nu_{electrolyte}}{\kappa} u = -\Delta p \quad (13)$$

Here, ρ and ν are density and kinematic viscosity of electrolyte that are calculated as mass-weight average of the ions in the electrolyte.

$$\rho_{electrolyte} = \sum \frac{c_i}{c_{total}} \mu_i \quad (14)$$

$$\nu = \sum \frac{c_i}{c_{total}} \nu_i \quad (15)$$

Here, the subscript i represents all vanadium ions, protons, sulfuric acid, and water. Densities of vanadium ions are presented in Table 1. Kinematic viscosity of each vanadium ion can be obtained using Stokes-Einstein relation [22]

$$\nu_i = \frac{k_B T}{6 D_i \pi r_{H,i}} \quad (16)$$

Here, k_B is Boltzmann's constant, $1.38 \times 10^{-23} m^2 kg/s^2 K$, and T is temperature. $r_{H,i}$ is Stokes radius for vanadium ions that are listed in Table 1. κ is permeability of a porous medium that is described by Kozeny-Carman equation.

$$\kappa = \frac{d_f^2 \varepsilon^2}{K_{CK}(1-\varepsilon)^2} \quad (17)$$

d_f is the fiber diameter of electrode, and K_{CK} is the Carman-Kozeny constant that determines the characteristics of flow field in porous media.

Table 1
Geometric and structural parameters of cell used in this study.

Parameters	Value
Width of the membrane	0.127 mm
Width of the electrode	3 mm
Width of the current collector	2 mm
Breadth of the electrode	20 mm
Height of the electrode	20 mm
Porosity of the electrode	0.67
Volume of the reservoir	15 mL
Diffusivity of vanadium ions ($V^{2+}/V^{3+}/V^{4+}/V^{5+}$)	8.768×10^{-12} / 3.222×10^{-12} / 6.825×10^{-12} / 5.897×10^{-12} m^2/s [28]
Density of vanadium ions ($V^{2+}/V^{3+}/V^{4+}/V^{5+}$)	3.357 / 4.571 / 4.87 / 5.76 g/cm^3 [29]
Stokes radius of vanadium ions ($V^{2+}/V^{3+}/V^{4+}/V^{5+}$)	0.32 / 0.32 / 0.21 / 0.28 nm [30]

The changes of the proton concentration during charge are considered as follows:

$$\varepsilon V_e \frac{dC_{H^+}}{dt} = \varepsilon Q(C_{H^+}^{res} - C_{H^+}) + \begin{cases} A_e \frac{j}{F} & (-)electrode \\ -(A_e - 2A_s)\frac{j}{F} & (+)electrode \end{cases} \quad (18)$$

Concentration changes of water can be calculated as follows; for the anode, we considered convection and electro-osmotic drag, while electrochemical reactions are additionally considered for the cathode.

$$\varepsilon V_e \frac{dc_{H_2O}}{dt} = \varepsilon Q(C_{H_2O}^{res} - C_{H_2O}) + \begin{cases} A_e n_d \frac{j}{F} & (-)electrode \\ -(A_e n_d + A_s)\frac{j}{F} & (+)electrode \end{cases} \quad (19)$$

Here, $n_d$is the proton drag coefficient. Changes of the ion concentration during discharge can be obtained by using a negative current density value. The concentration of each ion at the reservoir is expressed as a function of the flow rate and the concentration difference between the cell and reservoir.

$$\frac{dC_i^{res}}{dt} = \varepsilon \frac{Q}{V_{res}}(C_i - C_i^{res}) \quad (20)$$

Here, V_{res} is the reservoir volume. Cell voltage is then calculated as:

$$E_{cell} = E_{cell}^{rev} - \sum_k (IR)_k - \sum_k |\eta_a| \quad (21)$$

where E_{cell}^{rev} is the reversible open circuit voltage shown in follow [23].

$$E_{cell}^{rev} = E_{ca} - E_{an} + E_m \quad (22)$$

E_{ca} and E_{an} are open circuit potential for cathode and anode that are expressed as follow.

$$E_{ca} = E_{ca}^0 + \frac{RT}{F}\ln\left(\frac{C_{V(V)} \cdot (C_{H^+,ca})^2}{C_{V(IV)}}\right) \quad (23)$$

$$E_{an} = E_{an}^0 + \frac{RT}{F}\ln\left(\frac{C_{V(III)}}{C_{V(II)}}\right) \quad (24)$$

E_m is a Donnan potential across the membrane due to the differences in proton activities

$$E_m = \frac{RT}{F}\ln\left(\frac{C_{H^+,ca}}{C_{H^+,an}}\right) \quad (25)$$

$\sum_k (IR)_k$ is total ohmic loss containing the resistance of the membrane, electrode, and current collector; and η_a is the activation overpotential with contribution from each electrode that are shown below [21].

$$\eta_{ca} = \frac{2RT}{F} a\sinh\left(\frac{j}{2Fk_{ca}\sqrt{C_{V(IV)}C_{V(V)}}}\right) \quad (26)$$

$$\eta_{an} = -\frac{2RT}{F} a\sinh\left(\frac{j}{2Fk_{an}\sqrt{C_{V(III)}C_{V(II)}}}\right) \quad (27)$$

Here, k_{ca} and k_{an} are the reaction rate constant for each electrode that are shown follow.

$$k_{ca} = k_{ca,ref}\exp\left(\frac{FE_{ca}^0(T_{ref})}{R}\left[\frac{1}{T_{ref}} - \frac{1}{T}\right]\right) \quad (28)$$

$$k_{an} = k_{an,ref}\exp\left(-\frac{FE_{an}^0(T_{ref})}{R}\left[\frac{1}{T_{ref}} - \frac{1}{T}\right]\right) \quad (29)$$

The performance of a VFB can be assessed using various efficiencies, as defined below [24]:

$$Coulomb\ efficiency = \frac{Discharge\ capacity\ (Ah)}{Charge\ capacity\ (Ah)} \times 100\% \quad (30)$$

Table 2
Specifications related with pump system used in this study.

Parameters	Value
Viscosity of the electrolyte	4.928×10^{-3} Pa s [9]
Diameter of pipe	5.2 mm
Length of pipe	660 mm
Fiber diameter	17.6×10^{-3} mm
Kozeny-Carman constant	4.28 [23]
Pump efficiency	0.9 [31]

$$Energy\ efficiency = \frac{Discharge\ energy\ (Wh)}{Charge\ energy\ (Wh)} \times 100\% \quad (31)$$

$$Voltage\ efficiency = \frac{Energy\ efficiency}{Coulombic\ efficiency} \times 100\% \quad (32)$$

In this paper, we included power consumption by the pump to examine the VFB system efficiency according to the flow rate. The pump power consumption was calculated as a function of the pressure drop in the pipe, flow rate, and pump efficiency, which are listed in Table 2 and based on previous studies [25].

$$P_{pump} = \frac{\Delta P_{total} Q}{\alpha} \quad (33)$$

The total pressure drop, ΔP_{total}, in the VFB system is the sum of the pressure drop in the pipe and the electrode, and α is the pump efficiency. We assumed that the flow is laminar and incompressible. The pressure drop in the electrode is obtained using Darcy's law based on flow rate, characteristics of electrode and electrolyte [26].

$$\Delta P_{electrode} = \left(\frac{L_m}{w_m}\right)\frac{\nu_{electrolyte} Q}{\kappa t_m} \quad (34)$$

Here, L_m and w_m are the length and width of electrode. κ is the electrode permeability, and μ is the viscosity of electrolyte. The pressure drop in the pipe can be calculated using the Hagen-Poiseuille equation that are given as follow [26].

$$\Delta P_{pipe} = \frac{128\mu_{electrolyte} L_m Q}{\pi D_h^4} \quad (35)$$

where D_h is the hydraulic diameter of the flow channel. Modeling the system was conducted using the SIMULINK software package.

2.2. Experiment

The experimental setup was designed to investigate the steady and transient responses of the VFB system and demonstrate its operating strategy. A Nafion® 115 membrane was used to separate the electrolytes for the different electrodes with an active area of 20 × 20 mm^2. Carbon felt (SGL group, GFD4.6 EA) was used as the electrode with an approximate compression ratio of 30%. The electrodes were soaked in 3 M H_2SO_4 for 24 h and then dried in a vacuum oven at 30 °C. Next, they were heated at 400 °C for 30 h to functionalize their surface. A Viton gasket surrounded the electrode to seal the electrolytes. A copper current collector (70 × 40 × 2 mm) was placed next to the electrode to transfer electrons to a potentiostat (BioLogic, SP-150) for measurement. The electrolyte comprised 1.6 M V^{3+} and 1.6 M V^{4+} in 3 M H_2SO_4 solutions with 10 mL at each reservoir. A pump (ISMATIC) circulated the anolyte and catholyte between the cell and reservoir. Paraffin oil was used at the negative electrode to prevent the oxidation of V^{2+}.

Normally, the flow of electrolyte is supplied more than is predicted theoretically because an over-supplied electrolyte can supply more active material and prevent a deficiency of reactants at exit. In order to analyze the characteristics of the system according to over-supplied flow rate regardless of the system scale, the stoichiometric number, λ, is introduced as dimensionless parameter, which is the ratio of the actual

consumption to the theoretical consumption. Here, the theoretical reactant consumption and stoichiometric number are calculated as follows [27]:

$$Q_{theo} = \frac{I}{n \times F \times C \times SOC_{\min}} \tag{36}$$

$$\lambda = \frac{Q_{real}}{Q_{theo}} \tag{37}$$

where I is the current; n is the number of electrons transferred during the reaction, which is 1 for VFB; C is the total vanadium concentration for each reservoir (1.6 M); and SOC_{min} is the minimum state of charge, which is 20% in this study. In this study, the flow rate is varied from 1 to 9 mL/min, and the cut-off voltages of charging and discharging were 1.6 V and 1.0 V, respectively.

3. Results and discussion

Analysis of the VFB system began with validating the developed system model by comparing the experimental data. Through the model we could understand the effect of flow rate, current density, and size of active area on variation of ion concentration in VFB. Moreover, we could analyze the transient responses of the VFB system at different flow rates and current densities. Lastly, we suggested and demonstrated the optimal operation strategy for the VFB system by controlling the flow rate at different SOC values to improve the system's performance and efficiency for various scales of system.

3.1. Model validation

The developed model was validated by comparison between the calculated cell voltages and the measured values; the former is drawn as lines in Fig. 3 whereas the latter is represented as symbols. The current density was 100 mA/cm^2 at a constant flow rate of 6.5 mL/min. As summarized in Table 3, the fitting parameters, such as, specific surface per unit volume of the bulk electrode, rate constant for reaction at negative electrode, and ionic conductivity of the electrolyte, were used in this model to match calculations to experiment [21]. The simulated results show good agreement with the experimental results within an average error range of 3%. It is reasonable to conclude that the developed numerical model can be used to explain the experimental results and is suitable for quantitative analysis.

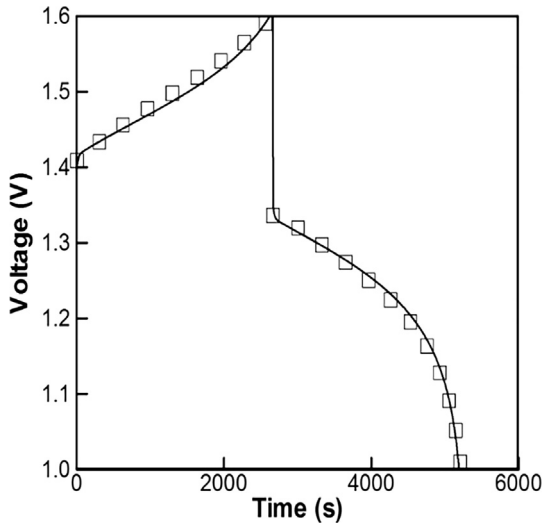

Fig. 3. Model validation at current density of 100 mA/cm^2 with flow rate of 6.5 mL/min: line (model), symbol (experiment).

Table 3
Fitted parameters for the model used in this study [21].

Parameters	Value
Specific surface per unit volume of the bulk electrode are for reaction	805 m^{-1}
Rate constant for reaction at negative side	4.527 × 10^{-6} m/s
Ionic conductivity of the electrolyte	120 S/m

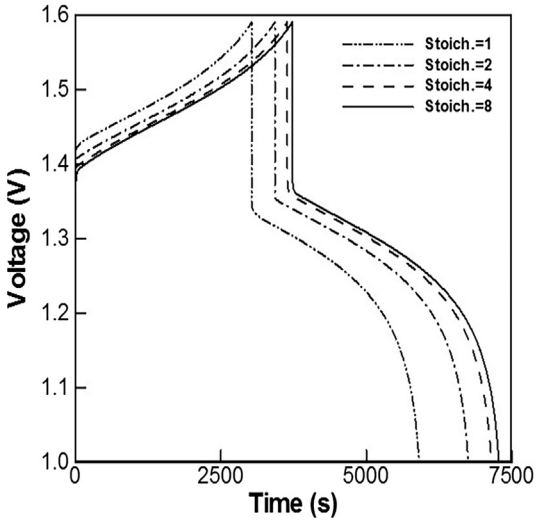

Fig. 4. Variation of charge–discharge curve with various flow rates.

3.2. Steady response analysis

In this section, we are going to analyze the effect of mass flow rate, current density, and size of active area on the changes of ion concentration in the electrode in steady state.

The charge–discharge behavior as a function of the stoichiometric number is shown in Fig. 4. The current density is maintained at 75 mA/cm^2 for the steady response analysis of the VFB system. As seen, the charge–discharge cycle time increases as the stoichiometric number increases. The extension of the cycle time can be explained as the increase in capacity of the VFB, which means that the battery can store more energy. However, the cycle time increment is saturated after a stoichiometric number of 4. These results indicate that optimal flow rate conditions are possible in an operating VFB system.

Changes of the charge–discharge cycle time can be explained by examining the variation of ion concentration. The concentrations of V^{2+} and V^{3+} at the negative electrode according to stoichiometric number are shown in Fig. 5(a) and (b), respectively. The concentration of V^{2+} ions increases during charge and decreases during discharge; in contrast, the V^{3+} ions move in the opposite direction. The ion concentration at the end of the charge–discharge cycle depends on the stoichiometric number; when this number is 1, the charge–discharge cycle ends at a SOC of 20%, but the cycle ends at a SOC of 10% when the stoichiometric number is 8. The change of the SOC at the electrode is caused by mixing the electrolyte between the electrode and reservoir; that is, larger flow rates greatly affect the ion concentration at the electrode by way of the ion concentration at the reservoir. During the charge process, the concentration of V^{2+} at the reservoir is lower than that at the electrode; as the flow rate increases, the influence of the reservoir increases and the concentration of V^{2+} at the electrode decreases. The changes of SOC at the end of cycle significantly affect the overpotentials at the beginning of the charge and discharge processes, and it changes start voltage of VFB. Therefore, the cycle time is changed according to flow rate. As the flow rate increases the coulomb efficiency decreases and voltage efficiency increases. Based on both factors, we

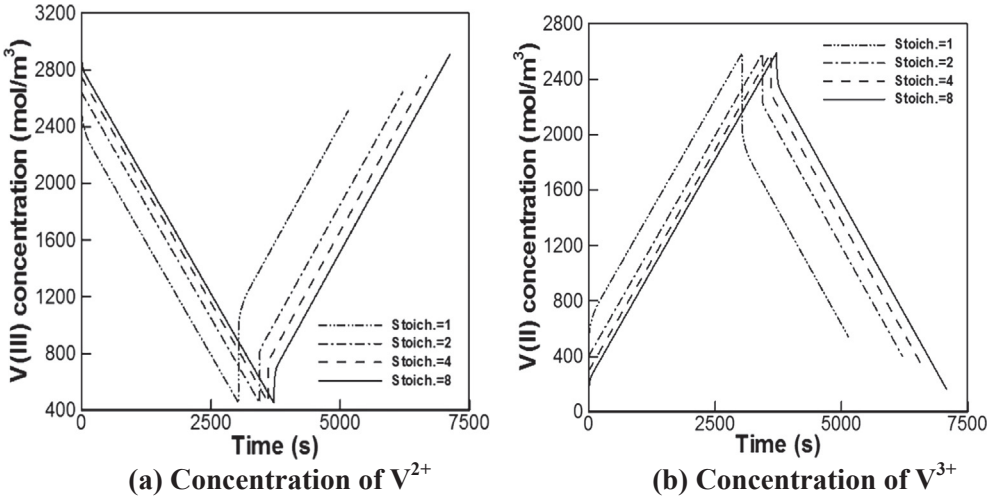

Fig. 5. Variation of concentration at negative electrode according to flow rates in steady state.

can know that energy efficiencies slightly increase from 78% to 80% according to flow rate.

Next, we examined the effect of current density on charge–discharge behavior. The changes of charge–discharge curve with various current densities are shown in Fig. 6. The current density is varied from 50 to 150 mA/cm^2 with constant stoichiometric number of 8. When the current density is over 150 mA/cm^2, the charge and discharge process cannot be operated due to overpotentials. As the current density increases, the charge–discharge cycle time decreases. When the current density increases from 100 to 150 mA/cm^2, the cycle time decreases from 4500 to 1800 s. Because of the shortened cycle time, the battery can store less energy. We can convince the reduction of capacity of the VFB by examining the variation of concentration of V^{2+} and V^{3+} ions during the cycle as current density increases that are shown in Fig. 7.

The gradient of concentration of V^{2+} ions during charge–discharge process increases as the current density increases. Because, the higher the current density, the faster the electrochemical reaction. On the other hand, the concentration of V^{2+} ions at the end of charge process decreases as the current density increases. When the current density increases from 50 to 150 mA/cm^2, the concentration of V^{2+} decreases of about 50%. This is due to the shortened charging time. Larger current density results in larger ohmic loss of membrane, it raises the start voltage of charge and drops the start voltage of discharge. Changed start voltage makes the operating voltage reach cut-off voltage of each process quickly. The shortened charge time give insufficient time to conversion of V^{3+} ions to V^{2+} ions during charge. Therefore, the concentration of V^{2+} ions at the end of charge process decreases as the current density increases. Due to shortened cycle time, the coulomb efficiency decreases. Increased start voltage also decreases the voltage efficiency. Therefore, the energy efficiency decreases from 82.7% to 63.2% according to the current density.

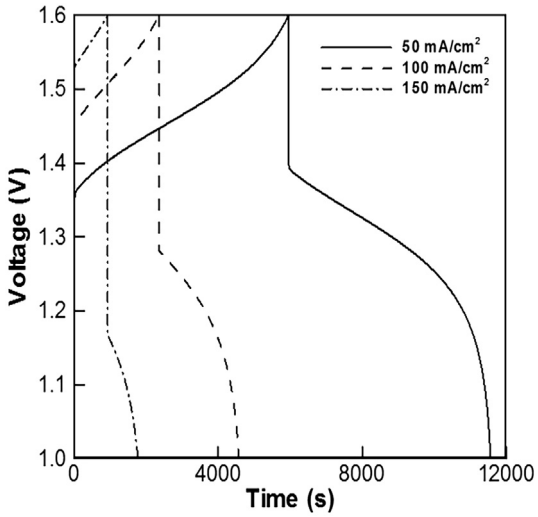

Fig. 6. Variation of charge–discharge curve with various current densities.

Lastly, we analyzed variation of charge–discharge process of VFB with various sizes of active area. The variation of charge–discharge curve for various sized VFB is expressed in Fig. 8. Here, the current density is 100 mA/cm^2, and the stoichiometric number is 8. Although the size of active area is different, the magnitude of start voltage is the same. The start voltage is determined by ohmic loss of membrane, and the ohmic loss is the same for various sizes of active area because the current density and membrane resistance are the same. Therefore, the start voltages of charge and discharge process are the same for various sizes of active area. On the other hand, the charge–discharge cycle time decreases as the size of active area increases. As active area increases from 36 to 100 cm^2, the cycle time decreases from about 950 to 650 s.

The changes of charge–discharge cycle time for various sized active area can be explained by analyzing the variation of concentration that is expressed in Fig. 9. The ion concentrations at the beginning and end of each process are almost the same, because the start voltage and cut-off voltage are the same. The gradient of ion concentration, however, is different according to sizes of active area. Large size of active area results in large current, and it means fast electrochemical reaction. Therefore, the bigger the size of active area, the larger the gradient of concentration, and we know that the VFB with large size of active area has the short cycle time. Although the cycle time decreases as size of active area increases, coulomb efficiency maintains constant, so does for voltage efficiency. Therefore, energy efficiencies of VFB with different sizes of active area are also similar whose value is about 77%.

3.3. Transient response analysis

It is important to examine the transient response of the VFB in order to suggest an operating strategy with variable flow rate during the charge–discharge cycle with different operating voltages.

First, the dynamic characteristics of the VFB cell were analyzed according to the change in stoichiometric number (i.e., from 1 to 2 and from 1 to 4) during the charge–discharge cycle with a SOC of 50% and a constant current density of 50 mA/cm^2. The responses of the cell voltage as a function of the stoichiometric number are shown in Fig. 10. When the stoichiometric number is increased (i.e., the flow rate is increased), the cell voltage drops while charging and rises while

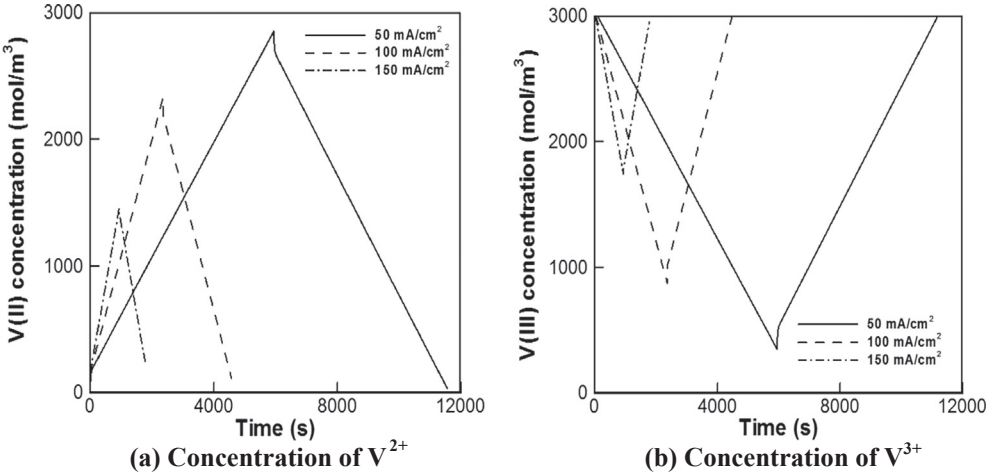

Fig. 7. Variation of concentration at negative electrode according to current densities in steady state.

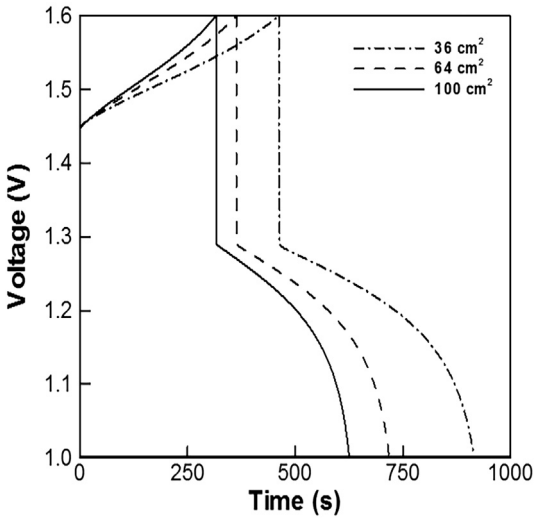

Fig. 8. Variation of charge–discharge curve of VFB with various sizes of active area.

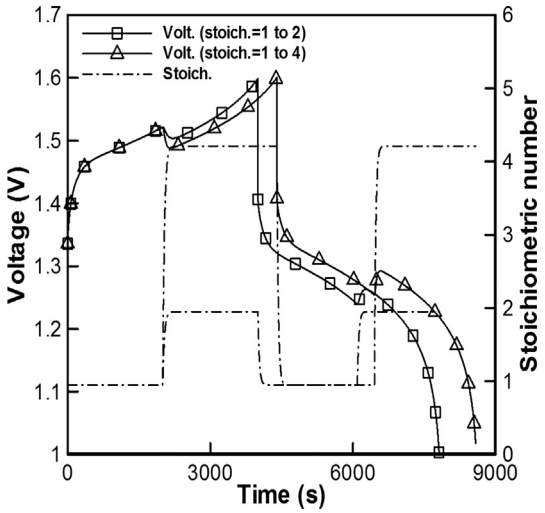

Fig. 10. Transient response of charge–discharge curve due to variable flow rate.

discharging; when stoichiometric number is increased from 1 to 2, the voltage drop during charge is 0.02 V and its rise during discharge is 0.024 V. When the stoichiometric number is increased from 1 to 4, the voltage drop during charge is 0.033 V and its rise during discharge is 0.038 V. Further, the cycle time increased as the stoichiometric number increased; the charge and discharge time increments are 400 s and 368 s, respectively. The changes in the cell voltage are related to changes in the vanadium ion concentration at each electrode.

Changes to the vanadium ion concentration at the negative

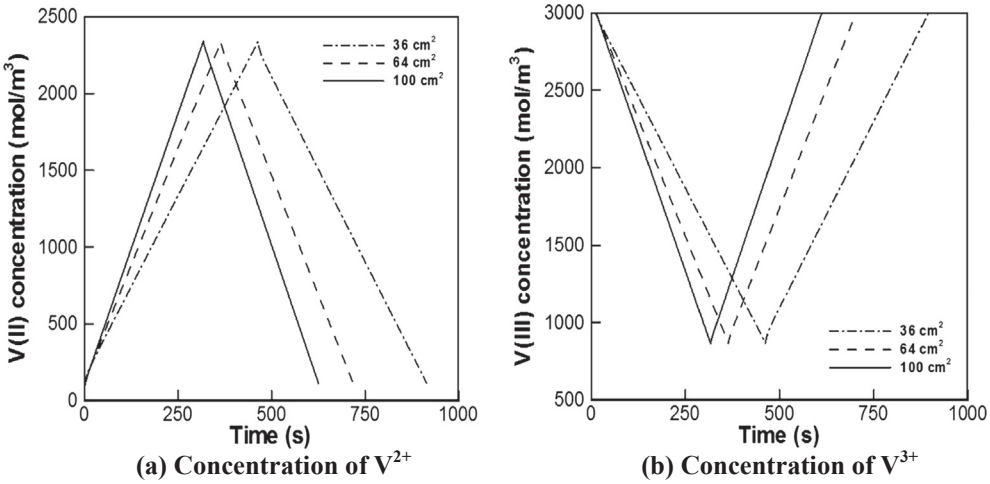

Fig. 9. Variation of concentration at negative electrode according to sizes of active area in steady state.

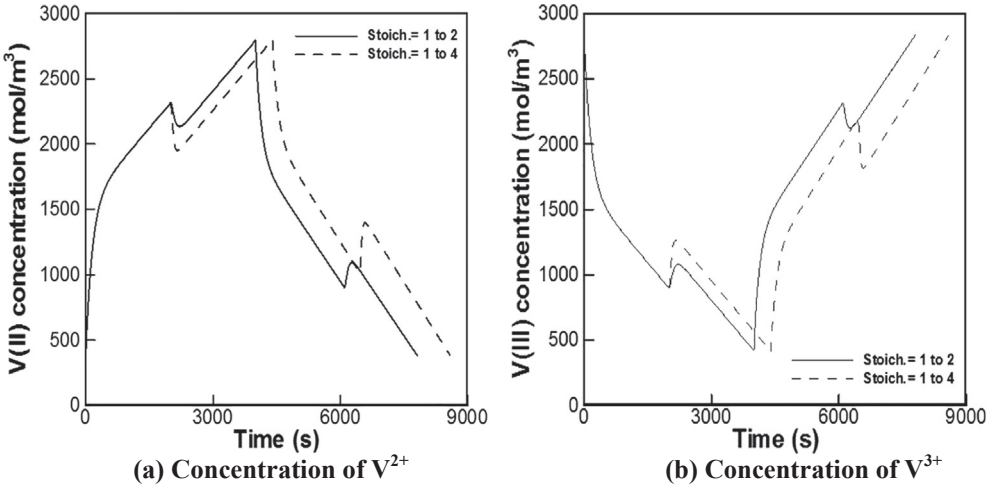

Fig. 11. Variation of concentration at negative electrode due to variable flow rate in transient state.

electrode as the stoichiometric number is changed are shown in Fig. 11. While charging, the V^{2+} ion concentration decreases and the V^{3+} ion concentration increases if the stoichiometric number increases. While discharging, the V^{2+} ion concentration increases and that of the V^{3+} ion decreases if the stoichiometric number increases. These changes result from changes to the mass flow rate. That is, more electrolyte with a lower concentration of V^{2+} ions stored in the reservoir enters the electrode as the mass flow rate increases during charge; consequently, the concentration of V^{2+} at the electrode becomes reduced. The change of the vanadium ion concentration leads to a change of the overpotential and thus changes the cell voltage.

The magnitude of the voltage change as the mass flow rate is changed is determined by the magnitude of the change in the vanadium ion concentration. As the flow rate is increased, the electrolyte circulation between the reservoir and electrode becomes faster, so their concentration difference becomes smaller, as shown in Fig. 12. Moreover, as the stoichiometric number increment is enlarged, the gap between the reservoir and electrode concentrations is reduced; during discharge, the concentrations are 356 mol/m^3 and 165 mol/m^3 when the stoichiometric number increases from 1 to 2 and from 1 to 4, respectively.

Next, we examined the transient response of charge–discharge curve due to variable current density that are shown in Fig. 13. The current density is changed from 50 to 100 mA/cm^2 and from 50 to 150 mA/cm^2 during the charge–discharge cycle with a SOC of 30% and a constant

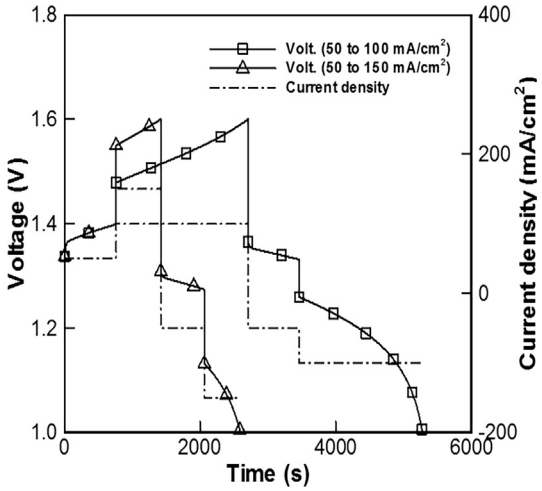

Fig. 13. Transient response of charge–discharge curve due to variable current density.

stoichiometric number of 8. When the operating current density is increased, the cell voltage rises during charge, and drops during discharge. When the current density is increased from 50 to 100 mA/cm^2, the increment of cell voltage while charging is about 0.08 V and the

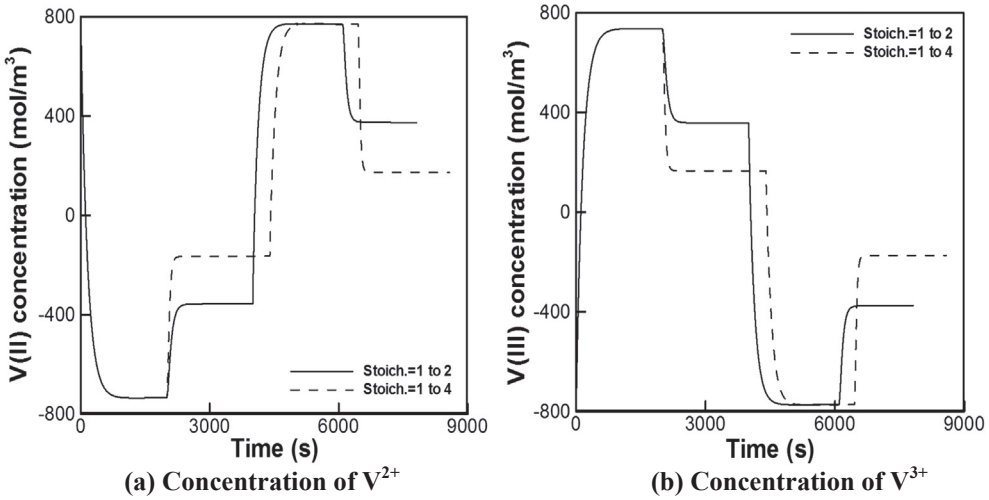

Fig. 12. Concentration difference between reservoir and electrode at negative side.

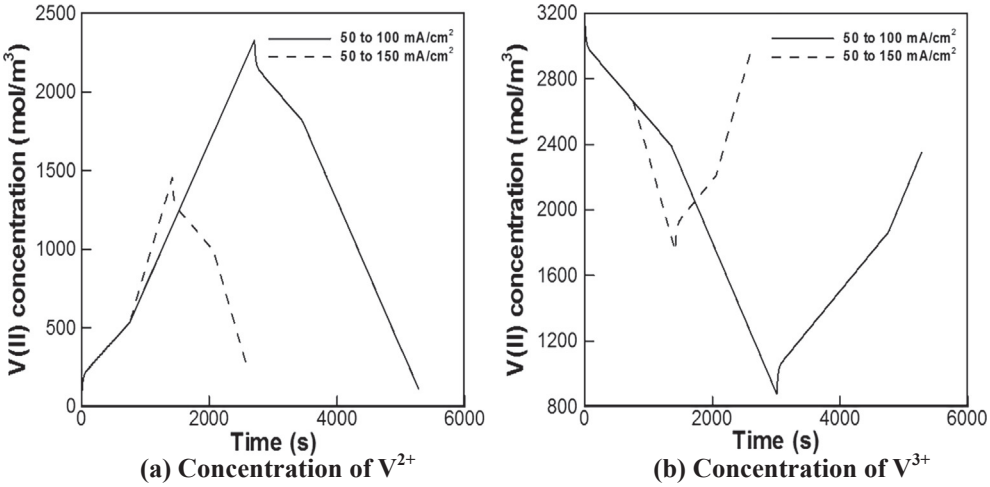

Fig. 14. Variation of concentration at negative electrode due to variable current density in transient state.

decrement while discharging is about 0.07 V. The larger the change of current density, the larger the change of cell voltage. The change of cell voltage shortens the charge–discharge cycle time. When the current density increases to 100 mA/cm^2, the cycle time is about 5200 s, but when the current density changes to 150 mA/cm2, the cycle is decreased to 2600 s. The shortened cycle time is resulted from the variation of ion concentration. The variation of concentration of V^{2+} and V^{3+} ions is expressed in Fig. 14. As mentioned in previous section, current density means the speed of reaction, and it is presented as the gradient of concentration–time graph. Therefore, the gradient of ion concentration increases as the current density increases. Due to the increase of gradient, the cycle time become reduced when the current density is increasing during charge–discharge process.

3.4. Optimal operation strategy for the VFB system

An optimal operating strategy for the VFB system can be suggested by adjusting the variable flow rate at an appropriate SOC. Using the concentrations of V^{2+} and V^{3+}, the SOC can be expressed as [23]:

$$SoC = \frac{C_{V(II)}}{C_{V(II)} + C_{V(III)}} = \frac{C_{V(V)}}{C_{V(V)} + C_{V(IV)}} \quad (38)$$

Here, we used concentrations of V^{2+} and V^{3+} at exit of the cell to prevent deficiency of reactant. The SOC at outlet is lower than that at inlet during charge and higher during discharge due to the electrochemical reaction of the vanadium ions in the cell. Therefore, we can operate VFB system safely by calculating the SOC using vanadium ions at outlet.

An energy efficiency map of the VFB system is drawn in Fig. 15 with stoichiometric numbers from 1 to 3 and SOC values from 20 to 80% at current densities of 50, 100, and 150 mA/cm^2. We first examined the effect changing the stoichiometric number. At a current density of 50 mA/cm^2, the energy efficiency of the VFB system is high with large changes of the stoichiometric number; the energy efficiency increases by 9% when the stoichiometric number is increased from 1 to 3 during charge–discharge. When the current density is 100 mA/cm^2, the maximum energy efficiency reaches 83% when the stoichiometric number is increased from 1 to 2.8. However, the energy efficiency gradient diminishes for higher stoichiometric numbers due to power consumption from the pump. This trend is also observed when the current density is 150 mA/cm^2. Energy efficiency reaches 78% when the stoichiometric number is increased from 1 to 2.5. As a results, the maximum energy efficiency is observed when the SOC is changed at an early stage. At 50 mA/cm^2, for example, optimal performance is achieved when the flow rate is changed from 1 to 3 at a SOC of 20%. Since the required flow rate is small in the lower current density region, the amount of additional power storage is much larger than the power consumption by the pump. When the current density is 100 mA/cm^2, the maximum energy efficiency is also obtained when the flow rate changes from 1 to 3 at a SOC of 20%. In case of 150 mA/cm^2, however, the maximum energy efficiency is observed when the flow rate changes from 1 to 3 at a SOC of 40%. Because the pump power consumption becomes larger when the current density is high, the maximum energy efficiency of the VFB system with a higher current density is lower by 4% than the former case.

Using the above results, we suggest the following empirical equation, which is a function of the current density, stoichiometric number, and SOC, to achieve the maximum energy efficiency for a VFB system.

$$eff_{Max} = -0.9j + 0.12\lambda - 1.62 \times 10^{-2}\lambda^2 + 1.58 \times 10^{-2}SOC - 3.1 \times 10^{-2}SOC^2 + 0.707 \quad (39)$$

Using this equation, the optimal strategy for maximizing energy efficiency for a VFB system can be obtained at all scales when the current density is less than 150 mA/cm^2. Fig. 16 displays the cell voltage with a constant current density of 75 mA/cm^2. As seen, the maximum efficiency is obtained when the stoichiometric number is increased from 1 to 2.85 at a SOC of 38%; the energy efficiency with various flow rates increased by 7.95% relative to the case of a stoichiometric number of 1. Through suggested equation, we can improve the performance of VFB system simply by changing operating conditions.

4. Conclusions

The steady and transient responses of an all-vanadium redox flow batteries (VFBs) are analyzed to understand the effect of parameters on the all-vanadium redox flow batteries performance and its energy efficiency. Based on the results, optimized operating strategies for the systems are suggested.

First, the performance of all-vanadium redox flow batteries at steady state is examined according to various mass flow rates (i.e., the stoichiometric number), current densities, and sizes of active area. As the stoichiometric number increases, the charge–discharge cycle time and the capacity of the flow battery also increase because higher stoichiometric numbers enhance the utilization of vanadium ions stored in the reservoir. Moreover, the increment of current density decreases the charge–discharge cycle time. Higher current density increases the ohmic loss due to resistance of membrane, and increases speed of electrochemical reaction. Therefore, the cycle time is reduced. Lastly the cycle time of the battery decreases as the size of active area

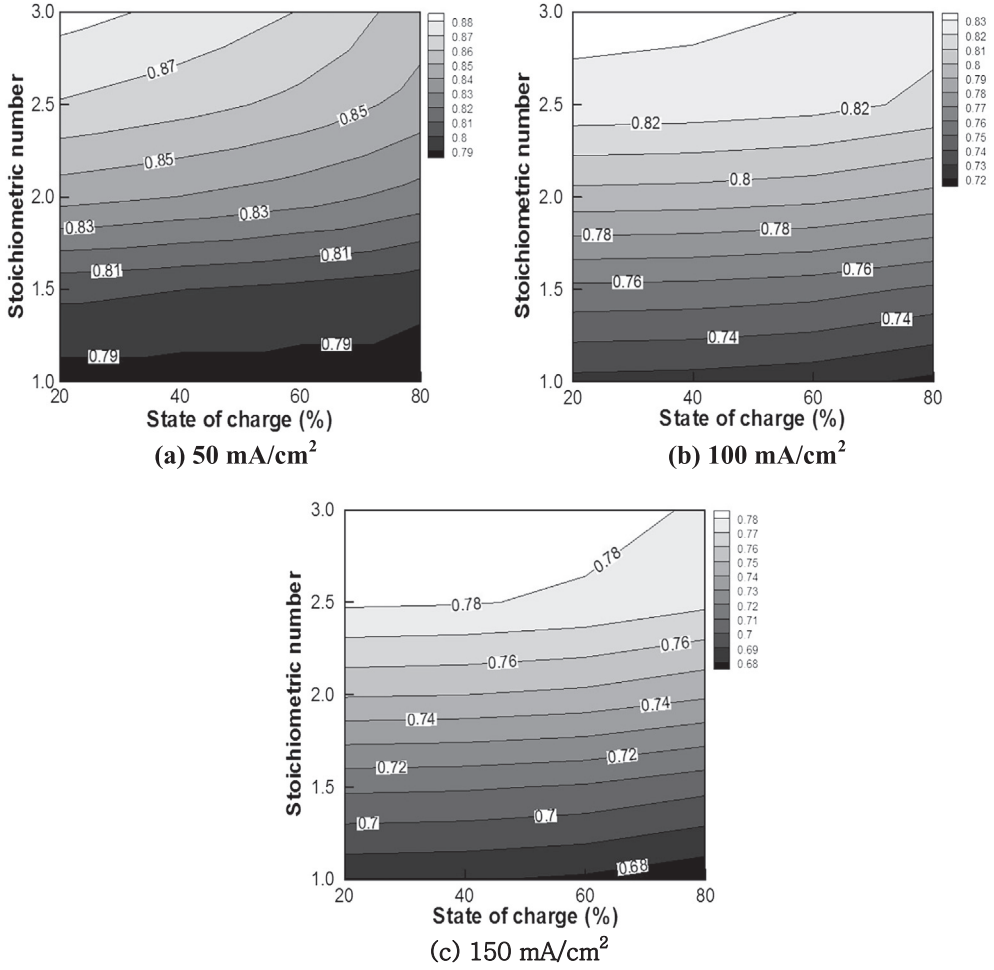

Fig. 15. Energy efficiency of the vanadium flow battery at different current densities.

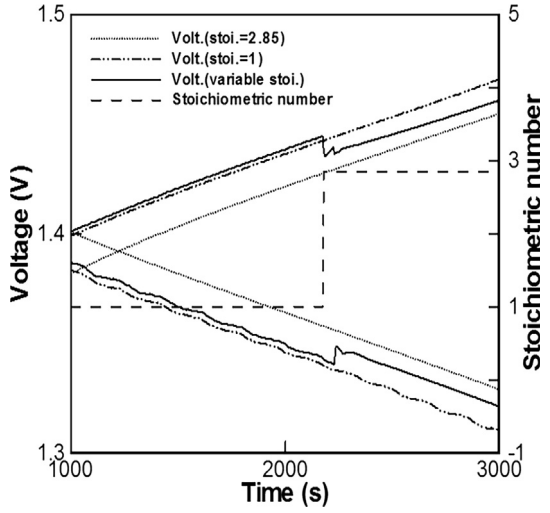

Fig. 16. Variation of the cell voltage followed by optimal operating strategy at 75 mA/cm^2.

increases. Because large size of active area increases current, and it raises speed of electrochemical reaction.

Next, the transient phenomena of the all-vanadium redox flow batteries system are examined as the mass flow rate was changed. Here, the flow rate is changed during the charge–discharge cycle with a state of charge of 50% and a constant current density of 50 mA/cm^2. When the stoichiometric number is increased from 1 to 2, the voltage drop during charge is 0.02 V and its rise during discharge is 0.024 V. By comparison, the voltage drop during charge is 0.033 V and its rise during discharge is 0.038 V when the stoichiometric number is increased from 1 to 4. This is because the concentration of vanadium ions at the electrode is influenced more strongly by the ion concentration in the reservoir at high flow rates. On the other hand, when the current density is changed from 50 to 100 mA/cm^2, the voltage rise is about 0.08 during charging, and its drop is about 0.07 V while discharge process. When the current density increases from 50 to 150 mA/cm^2, the voltage rise during charge is about 0.15 V, and its drop during discharge is 0.14 V. Increased ohmic loss and higher speed of electrochemical reaction results in the changes of voltage.

Lastly, the energy efficiency of the all-vanadium redox flow batteries system is investigated according to the stoichiometric number and state of charge. If the stoichiometric number increases from 1 to 3 at a state of charge of 20%, the energy efficiency increases from 78.6 to 88.2% at low current density. However, the energy efficiency decreases if the stoichiometric number is changed for higher state of charge values. At high current density, however, the maximum energy efficiency is achieved when the stoichiometric number increase occurs near the end of the charge–discharge processes, because of the relatively large power consumption of the pump. Based on these results, an empirical equation, which depends on the stoichiometric number and the state of charge, is suggested to maximize the energy efficiency of VFB systems. The energy efficiency is improved by 8% in the experimental setup simply by using the optimal operating strategy. It is expected that the energy efficiency of all scales of all-vanadium redox flow batteries systems will improve considerably by using the operating strategy

suggested in this study.

Acknowledgments

This research was supported by the Basic Science Research Program through the National Research Foundation of Korea, Korea funded by the Ministry of Science, ICT & Future Planning (NRF-2016R1A6A3A03007749). Additional support was provided by basic research project funded by Korea Institute of Science and Technology Europe and 'GO-KRICT' project funded by Korea Research Institute of Chemical Technology, Korea.

References

[1] Weber AZ, Mench MM, Meyers JP, Ross PN, Gostick JT, Liu Q. Redox flow batteries: a review. J Appl Electrochem 2011;41:1137–44.
[2] Li L, Kim S, Wang W, Vijayakumar M, Nie Z, Chen B, et al. A stable vanadium redox flow battery with high energy density for large scale energy storage. Adv Energy Mater 2011;1:394.
[3] Kazacos M, Cheng M, Skyllas-Kazacos M. Vanadium redox cell electrolyte optimization studies. J Appl Eletrochem 1990;20:463–7.
[4] Chen R, Hempelmann R. Ionic liquid-mediated aqueous redox flow batteries for high voltage applications. Electrochem Commun 2016;70:56–9.
[5] Zhou XL, Zeng YK, Zhu XB, Zhao TS. A high-performance dual-scale porous electrode for vanadium redox flow batteries. J. Power Sources 2016;325:329–36.
[6] Zhou XL, Zhao TS, Zeng YK, An L, Wei L. A highly permeable and enhanced surface area carbon-cloth electrode for vanadium redox flow batteries. J Power Sources 2016;329:249–54.
[7] Jang J, Kim T, Yoon SJ, Lee JY, Lee J, Hong YT. Highly proton conductive, dense polybenzimidazole membranes with low permeability to vanadium and enhanced H_2SO_4 absorption capability for use in vanadium redox flow batteries. J Mater Chem A 2016;4:14342–5.
[8] Latha TJ, Jayanti S. Ex-situ experimental studies on serpentine flow field design for redox flow battery system. J Power Sources 2014;248:140–6.
[9] Aaron DS, Liu Q, Tang Z, Grim GM, Papandrew AB, Turhan A, et al. Dramatic performance gains in vanadium redox flow batteries through modified cell architecture. J Power Sources 2012;206:450–3.
[10] Xu Q, Zhao TS, Leung PK. Numerical investigations of flow field designs for vanadium redox flow battery. Appl Energy 2013;105:47–56.
[11] Chang T, Zhang J, Fuh Y. Electrical, mechanical and morphological properties of compressed carbon felt electrodes in vanadium flow battery. J Power Sources 2014;245:66–75.
[12] Zhou XL, Zhao TS, Zeng YK, Yan XH. A vanadium redox flow battery model incorporating the effect of ion concentrations on ion mobility. Appl Energy 2015;258:157–66.
[13] Wei Z, Tseng KJ, Wai N, Lim TM, Skyllas-Kazacos M. Adaptive estimation of state of charge and capacity with online identified battery model for vanadium redox flow battery. J Power Sources 2016;332:389–98.
[14] Wei Z, Lim TM, Skyllas-Kazacos M, Wai N, Tseng KJ. Online state of charge and model parameter co-estimation based on a novel multi-timescale estimator for vanadium redox flow battery. Appl Energy 2016;172:169–79.
[15] Agar E, Benjamin A, Dennison CR, Chen D, Hickner MA, Kumbur EC. Reducing capacity fade in vanadium redox flow batteries by altering charging and discharging currents. J Power Sources 2014;246:767–74.
[16] Rahman F, Skyllas-Kazacos M. Vanadium redox battery: positive half-cell electrolyte studies. J Power Sources 2009;189:1212–9.
[17] Vijayakumar M, Li L, Graff G, Liu J, Zhang H, Yang Z, et al. Towards understanding the poor thermal stability of V^{5+} electrolyte solution in vanadium redox flow batteries. J Power Sources 2011;196:3669–72.
[18] Lee HJ, Choi NH, Kim H. Analysis of concentration polarization using UV-visible spectrophotometry in a vanadium redox flow battery. J Electrochem Soc 2014;161:A1291–6.
[19] Kim DK, Koh JS, Kim MS, Song HH. Experimental and computational study on the dynamic interaction between load variation and back pressure control in a polymer electrolyte membrane fuel cell for automotive application. Int J Hydrog Energy 2015;40:12370–1.
[20] Tang A, Bao J, Skylass-Kazacos M. Thermal modelling of battery configuration and self-discharge reactions in vanadium redox flow battery. J Power Sources 2012;216:489–91.
[21] Shah AA, Tangirala R, Singh R, Wills RG, Walsh FC. A dynamic unit cell model for the all-vanadium flow battery. J Electrochem Soc 2011;158:A671–7.
[22] Einstein A. Investigation on the Theoty of the Brownian movement. New York: Dover; 1926.
[23] Knehr KW, Kumbur EC. Opencircuit voltage of vanadium redox flow batteries: discrepancy between models and experiments. Electrochem Commun 2011;13:342–5.
[24] Ma X, Zhang H, Sun C, Zou Y, Zhang T. An optimal strategy of electrolyte flow rate for vanadium redox flow battery. J Power Sources 2012;203:153–8.
[25] Tang A, Bao J, Skyllas-Kazacos M. Studies on pressure losses and flow rate optimization in vanadium redox flow battery. J Power Sources 2014;248:154–62.
[26] McCabe W, Smith J, editors. Unit operations of chemical engineering, McGraw Hill Kogakusha Ltd., Tokyo; 1976.
[27] Merei G, Adler S, Magnor D, Leuthold M, Sauer DU. Multi-physics model for a vanadium redox flow battery. Energy Procedia 2014;46:194–203.
[28] Sun C, Chen J, Zhang H, Han X, Luo Q. Investigation on transfer of water and vanadium ions across Nafion membrane in an operating vanadium redox flow battery. J Power Sources 2010;195:890–7.
[29] https://www.sigmaaldrich.com/catalog/product/aldrich/.
[30] Oriji G, Katayama Y, Miura T. Investigations on V(IV)/V(V) and V(II)/V(III) redox reactions by various electrochemical methods. J Power Sources 2005;139:321–4.
[31] http://www.machinerylubrication.com/Read/28430/hydraulic-pump-motors-maintenance.

Glossary

Q: Flow rate (m^3/s)
j: Current density (mA/cm^2)
C: Concentration (mol/m^3)
A: Area (m^2)
ε: Porosity
w: Thickness (m)
V: Volume (m^3)
D: Diffusion coefficient (m^2/s)
t: Time (s)
n_d: Electro-osmotic drag
η: Overpotential (V)
P: Pressure (bar)
ρ: Density (kg/m^3)
ν: Viscosity (Pa s)
α: Pump efficiency

Subscripts

i: Ions
m: Membrane
e: Electrode
pipe: Pipe
electrolyte: Electrolyte